

# Counterflow of electrons in two isolated quantum point contacts

V.S. Khrapai,<sup>1,2</sup> S. Ludwig,<sup>1</sup> J.P. Kotthaus,<sup>1</sup> H.P. Tranitz,<sup>3</sup> and W. Wegscheider<sup>3</sup>

<sup>1</sup>*Center for NanoScience and Department für Physik, Ludwig-Maximilians-Universität, Geschwister-Scholl-Platz 1, D-80539 München, Germany*

<sup>2</sup>*Institute of Solid State Physics RAS, Chernogolovka, 142432, Russian Federation*

<sup>3</sup>*Institut für Experimentelle und Angewandte Physik, Universität Regensburg, D-93040 Regensburg, Germany*

We study the interaction between two adjacent but electrically isolated quantum point contacts (QPCs). At high enough source-drain bias on one QPC, the drive-QPC, we detect a finite electric current in the second, unbiased, detector-QPC. The current generated at the detector-QPC always flows in the opposite direction than the current of the drive-QPC. The generated current is maximal, if the detector-QPC is tuned to a transition region between its quantized conductance plateaus and the drive-QPC is almost pinched-off. We interpret this counterflow phenomenon in terms of an asymmetric phonon-induced excitation of electrons in the leads of the detector-QPC.

PACS numbers: 73.23.-b, 73.23.Ad, 73.50.Lw

The state of a confined quantum system is modified by interactions with an external field (or with external sources of energy). In semiconductor nanostructures the energy and quasi-momentum of electrons acting as probe are strongly influenced by the environment, e. g. via electron-electron or electron-phonon interaction. If driven out of equilibrium, Coulomb forces establish the local equilibrium within the electron system whereas electron-phonon interactions dominate the energy exchange with the environment [1]. Drag experiments in semiconductor nanostructures provide a tool to study the effect of external electrons or phonons onto a probe electron system.

Current drag between parallel two-dimensional (2D) electron layers has been investigated in GaAs/AlGaAs bilayer systems. At small interlayer separations, observations are consistent with the Coulomb drag phenomenon [2]. At larger separations virtual-phonon exchange has been invoked to explain the data [3]. A negative sign of a current drag between 2D and 3D electron gases in GaAs was explained by the Peltier effect [4]. At high filling factors in a perpendicular magnetic field a sign change of the longitudinal drag between parallel 2D layers was found as a function of the imbalance of the electron density in the two layers [5, 6].

Interactions between two lateral quantum wires in GaAs have been investigated in Ref. [7]. The observed frictional drag, strongly oscillating as a function of the one-dimensional (1D) subband occupation, was interpreted in terms of Coulomb interaction between two Luttinger liquids. Recently, the observation of negative Coulomb drag between two disordered lateral 1D wires in GaAs in perpendicular magnetic fields was reported [8].

Here we report on a novel interaction effect between two neighboring quantum point contacts (QPCs), embedded in mutually isolated electric circuits. When a strong current is flowing through the partially transmitting drive-QPC, we detect a small current in the second, unbiased, detector-QPC. The detector current flows in the *opposite* direction of the drive current and shows

a nonlinear dependence on the source-drain bias of the drive-QPC. It oscillates as a function of the detector-QPC transmission. We suggest an explanation of this counterflow phenomenon in terms of asymmetric phonon-induced excitation of ballistic electrons in the leads of the detector-QPC.

Our samples are prepared on a GaAs/AlGaAs heterostructure containing a two-dimensional electron gas 90 nm below the surface, with an electron density of  $n_S = 2.8 \times 10^{11} \text{ cm}^{-2}$  and a low temperature mobility of  $\mu = 1.4 \times 10^6 \text{ cm}^2/\text{Vs}$ . An AFM micrograph of the split-gate nanostructure, produced with e-beam lithography, is shown in the left inset of Fig. 1. The negatively biased central gate C divides the electron system into two separate circuits, and prevents leakage currents between them. Two QPCs are defined on the upper and lower side of the central gate, respectively, by biasing gates 8 and 3. Other gates are grounded if not stated otherwise.

The right inset of Fig. 1 shows a sketch of the counterflow experiment. We use separate electric circuits for the (upper) drive-QPC and (lower) detector-QPC. A dc bias voltage,  $V_{\text{drive}}$ , is applied to the left lead of the drive-QPC, while the right lead is grounded. A current-voltage amplifier with an input voltage-offset of about  $10 \mu\text{V}$  is connected to the right lead of the detector-QPC. Its left lead is always maintained at the same offset potential in order to assure zero voltage drop across the detector-QPC. In both circuits, a positive sign of the current corresponds to electrons flowing to the left. For differential counterflow conductance measurements, the drive bias is modulated at a frequency of 21 Hz and the resulting ac current component in the detector circuit is measured with lock-in detection in the linear response regime. All measurements are performed in a dilution refrigerator at an electron temperature below 150 mK. The experimental results are the same if detector and drive QPC are interchanged.

First, we characterize the QPCs using a standard differential conductance measurement. Figure 1 displays the differential conductances of both QPCs in linear re-

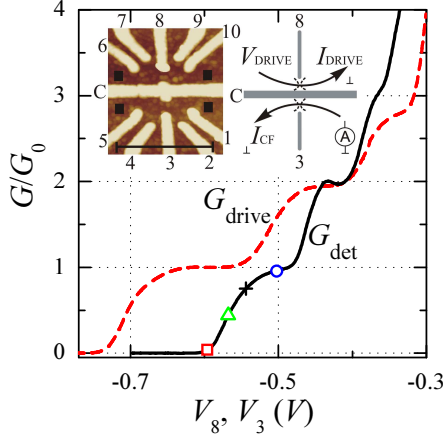


FIG. 1: Conductance of the drive-QPC (dashed line) and the detector-QPC (solid line) in the linear response regime as a function of respective gate voltages  $V_8$  and  $V_3$ . Symbols on the detector-QPC curve mark the  $V_3$  values used for counterflow conductance measurement presented in fig. 2b. Left inset: AFM micrograph of the metal gates on the surface of the heterostructure (bright tone). Black squares mark contacted 2DEG regions. The scale bar equals  $1 \mu\text{m}$ . Right inset: sketch of the counterflow measurement. The directions of currents are shown for the case of  $V_{\text{drive}} > 0$ .

sponse, measured as a function of the respective gate voltage  $V_3$ , or  $V_8$ . At low gate voltages, the QPCs are pinched-off and the conductance is close to zero. With increasing gate voltage, 1D channels successively open up [9]. For both QPCs we observe three conductance plateaus approximately quantized in units of  $G_0 = 2e^2/h$ . With high bias spectroscopy [10] we find the spacing between the two lowest subbands to be approximately 4 meV (3 meV) for the drive (detector) QPC. The energy window for opening a 1D subband is about 1 meV wide in both QPCs.

Having characterized the QPCs, we turn to counterflow measurements. Fig. 2a shows the dc counterflow current,  $I_{\text{cf}}$ , through the detector-QPC and the differential counterflow conductance,  $g_{\text{cf}} \equiv dI_{\text{cf}}/dV_{\text{drive}}$ , as a function of the bias on the drive QPC. Here, the drive-QPC is tuned to nearly half a conductance quantum  $G_{\text{drive}} = G_0/2$ , while the detector-QPC is in the pinch-off regime with  $G_{\text{det}} \simeq 10 \text{ G}\Omega^{-1}$ . Surprisingly, for  $|V_{\text{drive}}| \gtrsim 1 \text{ mV}$ , a finite current is observed in the unbiased detector circuit. The direction of  $I_{\text{cf}}$  is opposite to that of the drive-QPC current  $I_{\text{drive}}$ . The dc counterflow current is a threshold-like, nearly odd function of  $V_{\text{drive}}$ . Correspondingly, the differential counterflow conductance is negative and a nearly even function of  $V_{\text{drive}}$ . The sign of  $g_{\text{cf}}$  expresses a phase shift of  $\pi$  between the applied ac modulation of  $V_{\text{drive}}$  and the detected ac component of the counterflow current.

Figures 2c and 2d show the absolute value of  $I_{\text{cf}}$  for the nearly pinched-off detector as a function of the voltage on gate 8, which tunes the drive-QPC transmission. The corresponding drive-QPC differential conductance curves

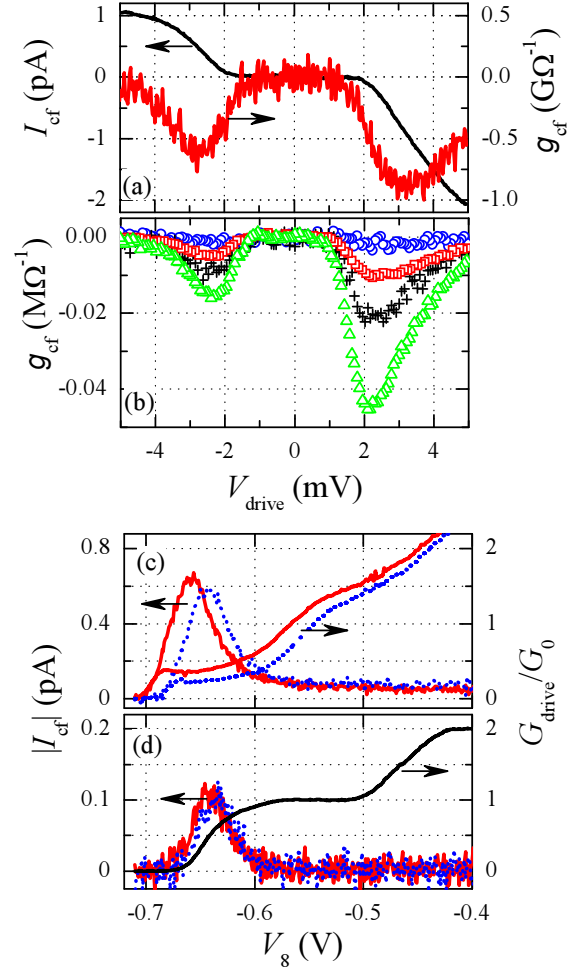


FIG. 2: (a) -  $I_{\text{cf}}$  and  $g_{\text{cf}}$  for the nearly pinched-off detector-QPC as a function of  $V_{\text{drive}}$ . (b) -  $g_{\text{cf}}$  measured for a set of  $G_{\text{det}}$  values marked by according symbols in fig. 1. (c,d) - Absolute value of  $I_{\text{cf}}$  as a function of the drive-QPC gate voltage  $V_8$ , for  $V_{\text{drive}} = \pm 4 \text{ mV}$  (c) and  $V_{\text{drive}} = \pm 2.25 \text{ mV}$  (d). Also shown is the drive-QPC's differential conductance at  $V_{\text{drive}} = \pm 4 \text{ mV}$  (c) and its conductance in linear response (d). Solid (dotted) lines correspond to  $V_{\text{drive}} < 0$  ( $> 0$ ). In (a),(b) gates 7 and 9 are grounded, while in (c),(d)  $V_7 = V_9 = -0.4 \text{ V}$ . The drive bias modulation used to measure  $g_{\text{cf}}$  is  $92 \mu\text{V rms}$ .

are also shown. For not too high  $V_{\text{drive}}$  (Fig. 2d), a non-zero counterflow current is only detected in the region between pinch-off and the first conductance plateau of the drive-QPC. For higher  $V_{\text{drive}}$  (fig. 2c)  $I_{\text{cf}}$  increases superlinearly with  $V_{\text{drive}}$  at its maximum and remains finite at higher gate voltages  $V_8$ . Since the source bias effects the potential distribution near the constriction, the nonlinear  $1/2$  conductance plateau of the drive-QPC shifts when changing  $V_{\text{drive}}$  [11]. This causes the shift of the extrema on Fig. 2c as well as the asymmetry of  $g_{\text{cf}}$  in Fig. 2a when reversing the bias.

We proceed to study the counterflow effect in the regime of a more opened detector-QPC. Figure 2b plots  $g_{\text{cf}}$  [12] as a function of  $V_{\text{drive}}$  for several values of  $G_{\text{det}}$

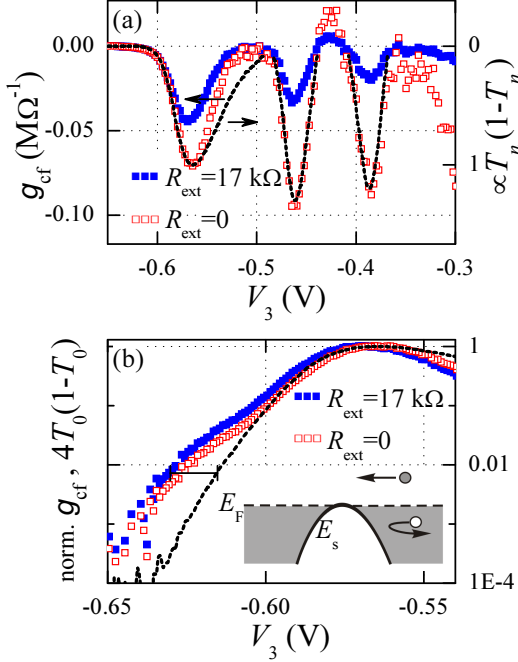


FIG. 3: (a)- Differential counterflow conductance as a function of the detector-QPC gate voltage. Filled symbols correspond to the  $g_{cf}$  measured at a finite external resistance  $R_{ext} = 17 \text{ k}\Omega$ , while open symbols show the corrected counterflow conductance  $R_{ext} = 0$  (see text). Also shown are the transmission functions  $\propto T_n(1 - T_n)$  for the three lowest 1D subbands of the detector-QPC (dashed lines), scaled to fit the corrected data. During the  $g_{cf}$  measurement the drive bias is modulated with a  $230 \text{ }\mu\text{V}$  rms signal about the mean value  $V_{drive} = +2.05 \text{ mV}$ . (b) - Normalized counterflow conductance (symbols as in (a)) and transmission function of the lowest 1D detector-QPC subband  $4T_0(1 - T_0)$  (dashed line) as a function of the detector gate voltage  $V_3$ . The scale bar shows a gate voltage interval corresponding to a change of the 1D subband energy by  $0.5 \text{ meV}$ . Inset: Sketch of possible scattering processes of nonequilibrium electrons and holes at a partially transmitting detector-QPC.

between 0 and  $G_0$  (marked with the same symbols in fig. 1). The qualitative appearance of  $g_{cf}(V_{drive})$  is independent of  $G_{det}$ . However, the amplitude of  $g_{cf}$  is a strongly non-monotonic function of the detector transmission. The counterflow conductance reaches its maximum for  $G_{det} \approx G_0/2$  and decreases rapidly with further increasing  $G_{det}$ . Note that the absolute value of  $g_{cf}$  is small, corresponding to a maximal ratio of the counterflow and drive currents  $|I_{cf}/I_{drive}| \lesssim 10^{-3}$ .

In Fig. 3a  $g_{cf}$  is plotted as a function of  $V_3$ , controlling the detector transmission.  $V_{drive}$  and  $V_8$  are adjusted for maximal  $g_{cf}$  and kept fixed. Confirming the trend seen in fig. 2b, the measured  $g_{cf}$  (solid symbols) strongly oscillates with increasing  $V_3$  and displays three pronounced maxima before the detector-QPC is fully opened. The position of the  $n$ -th maximum ( $n = 0, 1, 2$ ) is close to the value of  $V_3$ , where  $G_{det}/G_0 \simeq n + 0.5$  (Fig.1). Here, the bottom of the  $n$ -th 1D subband of the detector-QPC

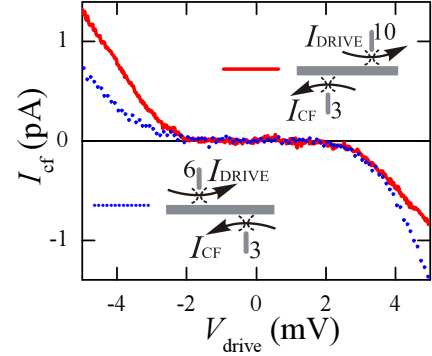


FIG. 4: Drive bias dependence of the counterflow current through the pinched-off detector-QPC for the drive-QPC formed with gate 6 (dotted line) or gate 10 (solid line). The detector-QPC conductance is about  $G_{det} = 5 \text{ G}\Omega^{-1}$ . The drive-QPCs are tuned to provide the maximal effect. Insets: sketches of the two counterflow measurements. The directions of currents are shown for the case of  $V_{drive} > 0$ .

aligns with the Fermi level of the leads. In contrast,  $g_{cf}$  is close to zero for fully transmitting 1D channels ( $G_{det}/G_0 \simeq n + 1$ ). The overall magnitude of  $g_{cf}$  decreases with increasing  $V_3$ , hence  $G_{det}$ . This is caused by a finite series resistance  $R_{ext}$  of the external circuit, which results in a measured  $g_{cf}$  lower than the case for an ideal ammeter [13]. The corrected counterflow conductance,  $g_{cf}^{ideal} \equiv g_{cf} \cdot (1 + R_{ext} \cdot G_{det})$ , corresponding to  $R_{ext} = 0$ , is shown in Fig. 3a with open symbols. The corrected maxima are roughly equal in size and symmetric. Moreover, the shape of the  $n$ -th maximum compares quite well with the corresponding function of the equilibrium transmission  $T_n(1 - T_n)$ , extracted from the detector conductance data  $T_n \equiv G_{det}/G_0 - n$  (dashed lines in Fig. 3a).

In figure 3b we plot the normalized  $g_{cf}$  and the transmission function  $4T_0(1 - T_0)$  on a logarithmic scale near the detector pinch-off. In the pinch-off regime the transmission probability of a QPC is expressed as  $T_0(E) \propto \exp([E - E_s]/\Delta)$  [11]. Here  $\Delta$  is the longitudinal curvature of the QPC's potential and  $E$  is the kinetic energy of current carrying electrons. The energy  $E_s$  of the 1D-subband bottom of the detector-QPC is controlled by gate 3 via  $E_s \propto -|e|V_3$ . This explains a nearly exponential drop of the transmission function with decreasing  $V_3$  (fig. 3b). In contrast, the measured  $g_{cf}$  drops considerably slower and remains finite even where the detector-QPC is already pinched-off in equilibrium. This experimentally observed excess contribution of the normalized  $g_{cf}$  versus  $T_0(E_F)$  signals that the counterflow current carrying electrons are excited well above the Fermi level. Converting the shift in gate voltage (see the bar in Fig. 3b) to energy, we find a characteristic excitation energy of  $E^* \approx 0.5 \text{ meV}$ . This is consistent with a recently reported  $1 \text{ meV}$  bandwidth excitation provided by the drive-QPC for electrons in a nearby double-dot quantum ratchet [14].

Next we study the counterflow effect between spatially shifted QPCs. Figure 4 shows  $I_{cf}$  through the nearly pinched-off detector-QPC as a function of the bias on the drive-QPC, which is formed either with gate 10 or gate 6, while gate 8 is now grounded (fig. 1). Despite the shift of the drive-QPC position relative to the detector-QPC by about 300 nm, the odd drive bias dependence of the counterflow current found in fig. 2 is practically preserved. This indicates that the excitation of electrons in one of the leads of the detector-QPC is not restricted to the close vicinity of the drive-QPC.

The current flowing through the pinched-off detector QPC is carried by ballistic electrons that have been excited in its leads. Hence, the oscillations of  $g_{cf}(V_3)$  in Fig. 3a can be explained in terms of the energy selectivity of the QPC transmission. Consider the transmission of nonequilibrium hot electrons and cold holes approaching the detector-QPC from the right lead. For  $|E_s - E_F| \gg E^*$  the transmission probabilities are equal for electrons and holes. However, for  $E_s \simeq E_F$  the  $T(E)$  energy dependence causes the electrons to be more likely transmitted to the left lead than the holes (inset to Fig. 3b), resulting in the oscillations of  $g_{cf}(V_3)$ . This mechanism is closely related to thermopower oscillations in QPCs [15, 16]. In contrast to thermopower measurements, in our case (i) current carrying electrons are not in thermal equilibrium and (ii) the energy source is an electrically separated drive circuit.

Our experimental results can be explained in terms of asymmetric phonon-based heating. The excess energy of current carriers in the drive circuit is mainly relaxed via emission of acoustic phonons, which, in turn, can be absorbed by electrons in the detector-QPC leads. In the linear transport regime average excess energies of cold holes in the source lead and hot electrons in the drain lead of the drive-QPC are the same. However, in the nonlinear regime this symmetry is broken, because of the

energy dependence of the transmission probability. As a result, non-equilibrium electrons with an excess energy  $\sim eV_{drive}$  are injected into the drain lead while the source lead with holes just below the Fermi level stays almost in thermal equilibrium [17]. In this situation acoustic phonons are predominantly emitted at the drain lead of the drive-QPC. The part of the phonons, which have momenta nearly parallel to the 2DEG plane, are preferentially absorbed in the adjacent lead of the detector-QPC, because of the device geometry [18]. The resulting imbalance between nonequilibrium electrons in the detector leads gives rise to the electric current directed opposite to that of the drive current.

In summary, we observe a current generated in an unbiased QPC and flowing in the opposite direction than the current in an adjacent strongly biased QPC. This counterflow current is most pronounced near pinch-off of the drive QPC. There, the drive-QPC behaves most strongly non-linear reflecting a large imbalance between electron and hole energies in its vicinity. This in turn results in a pronounced generation of non-equilibrium phonons near the drive-QPC, on its drain side. The strongly energy dependent absorption of these phonons occurs preferentially on the closeby lead of the detector-QPC. Between conductance plateaus of the detector-QPC, the resulting imbalance in the energy distribution of carriers near the detector-QPC causes the observed counterflow current.

The authors are grateful to V.T. Dolgoplov, A.W. Holleitner, C. Strunk, F. Wilhelm, I. Favero, A.V. Khaetskii, N.M. Chetelkatchev, A.A. Shashkin, D.V. Shovkun and P. Hänggi for valuable discussions and to D. Schröer and M. Kroner for technical help. We thank the DFG via SFB 631, the BMBF via DIP-H.2.1, the Nanosystems Initiative Munich (NIM) and VSK the Alexander von Humboldt foundation, RFBR, RAS, and the program "The State Support of Leading Scientific Schools" for support.

- 
- [1] V. F. Gantmakher and Y. B. Levinson, in *Carrier Scattering in Metals and Semiconductors* (North-Holland, Amsterdam, 1987)
  - [2] T.J. Gramila et al., *Phys. Rev. Lett.* **66**, 1216 (1991)
  - [3] T.J. Gramila et al., *Phys. Rev. B* **47**, 12957 (1993); H. Rubel et al., *Semicond. Sci. Technol.* **10**, 1229 (1995)
  - [4] B. Laikhtman et al., *Phys. Rev. B* **41**, 9921 (1990)
  - [5] X.G. Feng et al., *Phys. Rev. Lett.* **81**, 3219 (1998)
  - [6] J.G.S. Lok et al., *Phys. Rev. B* **63**, 041305 (2001)
  - [7] P. Debray et al., *J. Phys.: Condens. Matter* **13**, 3389, (2001); P. Debray et al., *Semicond. Sci. Technol.* **17**, R21, (2002)
  - [8] M. Yamamoto et al., *Science* **313**, 204, (2006)
  - [9] B.J. van Wees et al., *Phys. Rev. Lett.* **60**, 848 (1988); D.A. Wharam et al., *J. Phys. C* **21**, L209 (1988)
  - [10] A. Kristensen et al., *Phys. Rev. B* **62**, 10950 (2000)
  - [11] L.I. Glazman, A.V. Khaetskii *JETP Lett.* **48** 591 (1988)
  - [12] For increasing  $G_{det}$  the noises in the detector circuit increase, making the dc measurements very difficult.
  - [13] The input resistance of the I-V amplifier, the ohmic contacts and wiring resistances result in  $R_{ext} = 17$  k $\Omega$ . The validity of the above formula has been checked by applying an additional 47 k $\Omega$  resistor in series to  $R_{ext}$ .
  - [14] V.S. Khrapai et al., *Phys. Rev. Lett.* **97**, 176803 (2006)
  - [15] L.W. Molenkamp et al., *Phys. Rev. Lett.* **68**, 3765 (1992); H. van Houten et al., *Semicond. Sci. Technol.* **7**, B215 (1992)
  - [16] A.S. Dzurak et al., *J. Phys.: Condens. Matter* **5**, 8055, (1993)
  - [17] A. Palevski et al., *Phys. Rev. Lett.* **62**, 1776 (1989); for asymmetric heat production in 3D point contacts see U. Gerlach-Meyer, H.J. Queisser *Phys. Rev. Lett.* **51**, 1904 (1983)
  - [18]  $|I_{cf}|$  is reduced for  $V_{drive} < 0$  ( $> 0$ ) and the drive-QPC shifted to the lh (rh) side of the detector-QPC (fig. 4). This is understood in terms of absorption of phonons in both leads of the detector-QPC.